The low-field Hall effect, deviation from Matthiessen's rule and the two-group model for dislocated high-purity copper

1994 J. Phys.: Condens. Matter 6 11229

(http://iopscience.iop.org/0953-8984/6/50/029)

J. Phys.: Condens. Matter 6 (1994) 11229–11237. Printed in the UK

The low-field Hall effect, deviations from Matthiessen's rule and the two-group model for dislocated high-purity copper

F Sachslehner

Institut für Festkörperphysik der Universität Wien, Strudlhofgasse 4, A-1090 Wien, Austria

Received 18 August 1994, in final form 28 September 1994

Abstract. The low-field Hall effect at 4.2 K and deviations from Matthiessen's rule between 4.2 K and 140 K were studied for dislocated samples of high-purity copper. In the framework of the two-group model it is shown that for a good agreement between low-field Hall effect and DMR data it is necessary to take into account the different averaging of relaxation times for low-field Hall effect and electrical resistivity. The mathematical analysis used leads to a definition of neck angle in the two-group model.

1. Introduction

The physics of dislocations is an established field of modern physics and materials research [1]. However there is still a lack of information concerning the electronic transport properties of dislocated metals [2, 3]. At present there is no single accepted explanation of resistivity measurements in dislocated metals, which show considerable deviations from Matthiessen's rule (DMRs) [4, 5]. Recent theoretical work has suggested [6, 7] that the electrical resistivity of dislocations is proportional to the dislocation line length. This would lead to the important result that the electrical dislocation resistivity could be used as a measure of dislocation density [2, 4].

In general the 'true' dislocation resistivity ρ_d is 'hidden' by DMRs, which can have the same size as ρ_d itself. The DMRs are believed to be mainly produced by different anisotropy parameters of the various scatterers of the conduction electrons [4, 8]. Although it has been known for a long time that knowledge of scattering anisotropy is important [5, 8] a systematic study of it for the situation of electron–dislocation scattering—as could be done by the low-field Hall effect (LFHE)—has never been performed. This topic is of special interest, since Watts' model of electron–dislocation scattering gives a prediction of the detailed scattering anisotropy over the whole Fermi surface [6].

The idea of the present paper is to test the frequently used two-group model (TGM) of Ziman [9], as developed by Dugdale and Basinski [8] to explain DMR, by seeing whether it can consistently explain both LFHE and DMR in dislocated samples of high-purity copper. Several authors have tried to show the usefulness of the TGM [10–13]. Even in de Haas–van Alphen [14] and magnetic field induced surface state resonance [15] investigations discussions within the TGM were used for more or less successful comparison. However, especially in the context of dislocated samples the reliability of the TGM has never been tested systematically for LFHE and DMR together although both quantities react very sensitively to dislocations.

0953-8984/94/5011229+09$19.50

The common properties of the low-field Hall coefficient R_H and the DMR can be seen by the following TGM expressions according to [12] and to [8] and [16]:

$$-R_H = f(1 + A_1^2 a)/(1 + A_1 b)^2 \tag{1}$$

with A_1 as the scattering anisotropy parameter of what is assumed to be a single scatterer labelled 1 (see equations (5) and (9)). The terms a, b and f contain integrals involving velocity and curvature over the neck and belly regions of the Fermi surface (see subsection 3.3). By estimating a, b and f and defining the neck region of the Fermi surface to lie within a 20° cone about ⟨111⟩ Barnard [12] reduced equation (1) to

$$-R_H = 7.65 \times 10^{-11}(1 + 0.054A_1^2)/(1 + 0.257A_1)^2 \ (\mathrm{m^3\ C^{-1}}). \tag{2}$$

The DMR δ in a system of two scatterers (subscripts 1 and 2) can be written as (for three scatterers see [17])

$$\delta = \rho_1\rho_2(A_2 - A_1)^2 b^2/(A_1 b(1 + bA_2)^2\rho_2 + A_2 b(1 + bA_1)^2\rho_1) \tag{3}$$

where A_1 and A_2 are the scattering anisotropy parameters of the two scatterers and ρ_1 and ρ_2 are the resistivities of each scatterer on its own. Hence R_H and δ are linked by the anisotropy parameter A_1 and the integral term b. While the DMR measurement involves always at least two scatterers the great advantage of the LFHE is that it can be measured in the limit of only *one* dominating scatterer.

The present paper is based on the following concept (by applying the equations (2) and (3)): the Hall coefficient of a high-purity sample with high dislocation density measured at 4.2 K, $R_H^{4.2}$(dis), will give A_{dis}, the anisotropy parameter of electron–dislocation scattering. Then, additionally, the DMR can be studied as a function of temperature arising from dislocations and phonons as scatterers. A suitable anisotropy parameter for electron–phonon scattering above 100 K, A_{ph}, will be given by the room temperature Hall coefficient of copper, R_H^{300}(ph). Moreover, as a simplification in our high-purity samples the influence of the impurity resistivity ρ_{im} will be negligible when the deformation (i.e. the dislocation density) is large enough ($\rho_d \sim 10\rho_{im}$). Thus any anisotropy of impurity scattering may be neglected in the data analysis (subsection 3.2).

It should be mentioned that the low-field Hall coefficient R_H, being one component of the transport tensor, has the same values of electronic transport relaxation times as are involved in DMR and resistivity. Since in the present case electrical resistivity is mainly caused by large-angle scattering one should not use relaxation times obtained from the de Haas–van Alphen effect, which is equally sensitive to large- and small-angle scattering [4]. The experimental problems of making LFHE measurements in high-purity metals have already been discussed [11, 18].

2. Experimental details

The following paragraphs describe the sample materials of high-purity copper (in brackets the abbreviations used subsequently), the preparation procedures and the heat treatments used.

(i) Metalleurop (ME): 99.9999% pure copper ingot, weight 1 kg; slices of 1–2 mm were cut by a Buehler cutting wheel and polished; the slices were rolled to foils of about 200 μm thickness between copper sheets; annealing for 16 h at 500 °C in high vacuum (pressure always $< 1 \times 10^{-6}$ mbar). Resulting residual resistivity, 1.2 nΩ cm at a mean grain size of 160 μm.

(ii) MRC grade (MRC): 99.999% pure copper foils of 125 μm thickness; annealing for 11 h at 950 °C in high vacuum followed by oxygen annealing for 4 h at 950 °C at a dynamic pressure of 2.6×10^{-4} mbar. Resulting residual resistivity, about 0.6–0.8 nΩ cm (without oxygen annealing 3.4 nΩ cm) at a mean grain size of 260 μm.

(iii) Goodfellow (GF): 99.99% pure copper foils of about 250 μm thickness; annealing for 23 h at 950 °C in high vacuum followed by oxygen annealing for 10 h at 950 °C. Resulting residual resistivity, 0.6 nΩ cm (without oxygen annealing 5.5 nΩ cm) at a mean grain size of 170 μm,

(iv) Single crystal (SC): 99.95% commercial copper, grown by the Bridgman technique (in 5N purity argon atmosphere, pressure 260 mbar) from a rod with 6 mm diameter as a multislip crystal with 1×3 nm cross section. Residual resistivity in as-grown condition, 2.8 nΩ cm; after annealing for 11 h at 950 °C followed by 48 h oxygen annealing, 0.17 nΩ cm.

Different densities of dislocations were introduced into the annealed foils by tensile straining (from $\varepsilon = 0$ to 15%) or rolling (from true strain $\varepsilon = 13\%$ to 130%). The strain rate $\dot{\varepsilon}$ was 3×10^{-4} s^{-1} and in the case of the single crystal 1.5×10^{-4} s^{-1}. Vacancies were annealed out at room temperature. A separate foil was prepared for each deformation state.

The final samples were made by spark erosion with dimensions of 45 mm $\times$ 3 mm having two arms in the centre for Hall effect measurements (1 mm wide $\times$ 5 mm long) and two arms at a distance of 30 mm for resistivity measurements. The Hall voltage was measured by a SQUID picovoltmeter (resolution 1.5 pV Hz$^{-1/2}$), which has been described elsewhere [18]. The DMR measurements were performed in an evaporation cryostat [19] by the usual four-wire technique using a modern nanovoltmeter. The 'experimental dislocation resistivity' $\rho_{d,ex}$ as a function of temperature T was obtained by the relation $\rho_{d,ex}(T) = \rho(T, \varepsilon) - \rho(T, \varepsilon = 0)$, where $\rho(T, \varepsilon)$ and $\rho(T, \varepsilon = 0)$ are the resistivities of the dislocated sample and an undeformed reference sample, respectively. Thus $\rho_{d,ex}(T)$ is a measure of the experimental DMR as a function of temperature. The geometry factor G was determined for each sample in the annealed state by assuming [20] $G = [R(293\ \text{K}) - R(4.2\ \text{K})]/\rho_{ideal}(293\ \text{K})$, where $\rho_{ideal}(293\ \text{K}) = 1676$ nΩ cm [21] was used. The error of $\rho_{d,ex}(4.2\ \text{K})$ is 0.02 nΩ cm and that of $\rho_{d,ex}(130\ \text{K})$ is 0.2 nΩ cm.

In the case of the single crystal, current and potential leads where spot welded analogously to the arms of the polycrystalline samples. Hall effect and resistivity measurements (only at 4.2 K and at room temperature) were done on one and the same single crystal in a series of different deformation states (from $\varepsilon = 0$ to $\varepsilon = 7\%$).

3. Results and discussion

3.1. Hall effect

Figure 1 shows the Hall coefficient R_H at 4.2 K as a function of the ratio $\rho_{d,ex}(4.2\ \text{K})$ to impurity resistivity ρ_{im} for the four sets of copper samples investigated. The right-hand ordinate shows the R_H scale converted into A values according to equation (2). The following results can be seen:

(i) R_H of the undeformed samples varies from -6.82 (ME) to -5.84 (SC). This means the impurity scattering in these samples is anisotropic ($A \sim 0.6$ for SC) in contrast to the usual assumption that electron impurity scattering should be isotropic ($A = 1$) [22]. For the polycrystalline samples also some influence of electron–grain boundary scattering has to be taken into account. Larger magnitudes of R_H correspond to smaller grain sizes (see section 2).

Size effect corrections turned out to be negligible.

(ii) R_H reaches approximately the same value of -6.90 ± 0.05 for $\rho_{d,ex}/\rho_{im}$ near 10 or above. This shows that LFHE measurements yield a clear and well defined result for A_{dis} in the region of dominating electron–dislocation scattering, independent of the materials investigated.

(iii) In the region $0 < \rho_{d,ex}/\rho_{im} < 5$–10, R_H monitors a superposition of the anisotropy of scattering by impurities, dislocations and (apart from SC) grain boundaries. An estimation of the grain boundary resistivity by using the value $3.12 \times 10^{-12}\Omega$ m^2 [23] and the grain sizes of section 2 is about 0.2 nΩ cm for the ME and GF samples. Nevertheless the total area of grain boundaries may have a larger influence on R_H than the impurity content. This can be understood in the following way: grain boundaries may be considered to consist of arrays of dislocations and therefore their contribution to anisotropic scattering or to the Hall coefficient should behave in a similar manner to that of dislocations. The relatively small contribution of the grain boundaries to resistivity would become enlarged in the LFHE by the high dislocation-like anisotropy. This similarity between grain boundaries and dislocations could lead to the observed effect that R_H of the 'fine-grained' materials ME and GF is already approximately constant from $\rho_{d,ex}/\rho_{im} \sim 3$. The larger scatter of R_H values can be found only at deformations $0 < \varepsilon < 3\%$ and seems to stem from the individual grain boundary density near the Hall effect contacts of each sample.

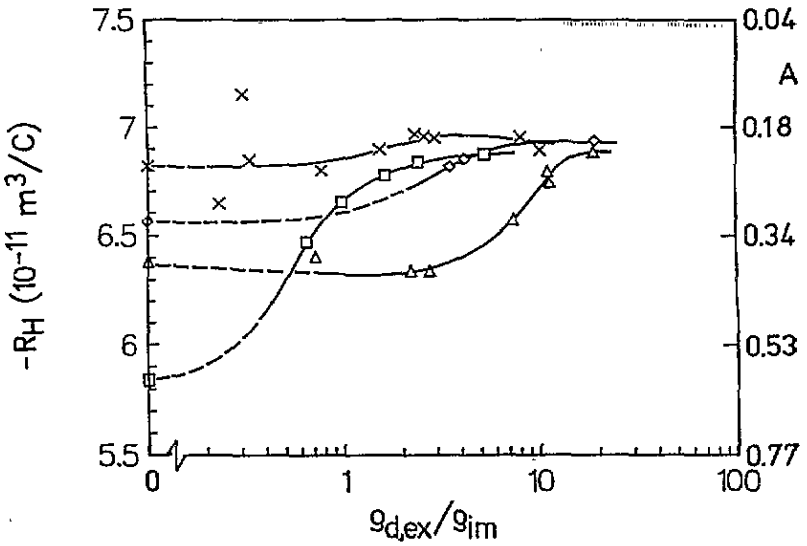

Figure 1. The Hall coefficient at 4.2 K, R_H, as a function of the ratio of experimental dislocation resistivity to impurity resistivity, $\rho_{d,ex}/\rho_{im}$. ×, ME copper; ◇, GF copper; △, MRC copper; □, SC copper. Values of ε (%) corresponding to the data points shown (always from the left to the right; R marks deformations made by rolling) are as follows: ME, 0, 1, 2, 3, 5, 10, 15, 13R, 16R, 34R, 49R; GF, 0, 13, 16, 36; MRC, 0, 5, 11, 11, 20R, 42R, 42R, 130R; SC, 0, 1, 2, 3, 4.6, 7.

3.2. DMR

The 'normalized' DMR data as a function of temperature can be seen in figure 2 for the ME and GF copper, where $D = \rho_{d,ex}(T)/\rho_{d,ex}(4.2\ K)$. The values of deformation ε and experimental dislocation resistivity $\rho_{d,ex}(4.2\ K)$ are indicated. The two curves shown are very similar and follow the behaviour shown in [22]. Further curves obtained for the ME copper ($\varepsilon = 35\%$, $\rho_{d,ex} = 10.63\ n\Omega\ cm$) and the GF copper ($\varepsilon = 36\%$, $\rho_{d,ex} = 11.52\ n\Omega\ cm$) are not shown, because they would be in the same range as the curves shown.

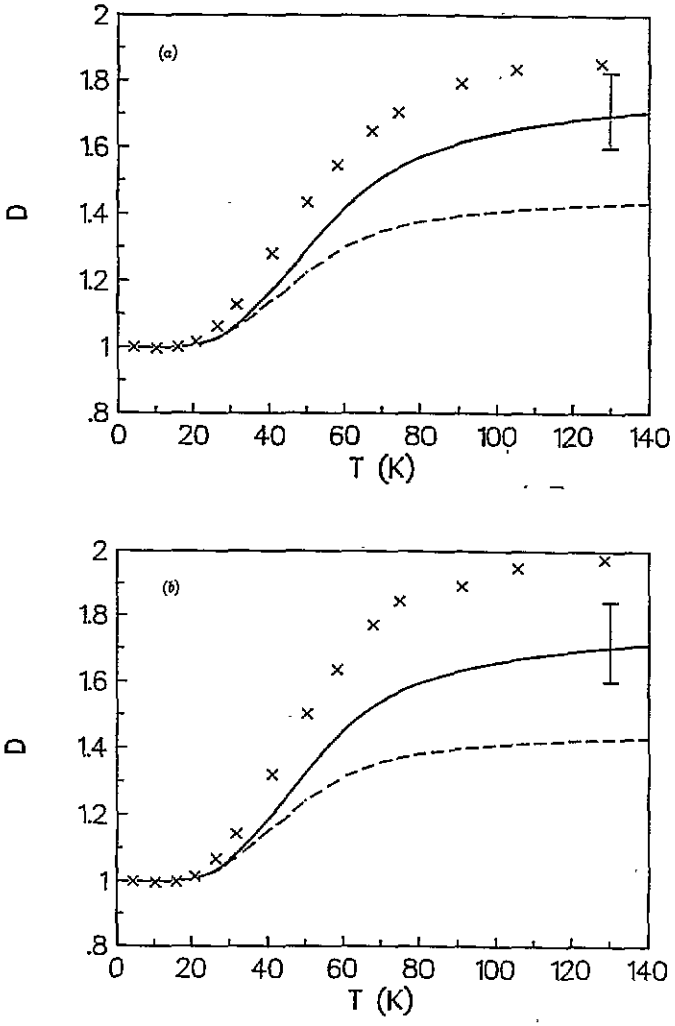

Figure 2. Normalized DMR curves ($D = \rho_{d,ex}(T)/\rho_{d,ex}(4.2\ K)$) as a function of temperature, T. ×, experimental points; — — —, Barnard's version, $A_{dis} = 0.21$ and $b = 0.257$; ——, exact version, $A_{dis} = 0.14$ and $b = 0.219$. (*a*) GF copper, $\rho_{d,ex}(4.2\ K) = 16.34\ n\Omega\ cm$, $\varepsilon = 82\%$; (*b*) ME copper, $\rho_{d,ex}(4.2\ K) = 13.29\ n\Omega\ cm$, $\varepsilon = 49\%$.

If we try to calculate theoretical curves by using equations (2) and (3) we have to keep in mind the following:

(i) Due to the relatively large ratio $\rho_{d,ex}/\rho_{im}$ we can assume $\rho_{d,ex}(4.2\ \mathrm{K}) \sim \rho_d(4.2\ \mathrm{K})$, where $\rho_d(4.2\ \mathrm{K})$ is the 'true' dislocation resistivity (see [22]).

(ii) For the same reason (as can be easily shown) we may omit impurity contributions and use equation (3) only for contributions of dislocations and phonons.

(iii) Above 100 K, where phonons are predominantly large-angle scatterers, we expect $A_{ph} \sim 1$, as assumed elsewhere [12, 24].

(iv) There exists some uncertainty for the values of A_{ph} between 4.2 K and 100 K because of significant small-angle scattering in that temperature range. For small-angle scattering no relaxation time or anisotropy parameter can be defined. Since these details of A_{ph} will determine only the transition from the low to the high level of the DMR curves and not the height at high temperatures we will use $A_{ph} \sim 1$ from 4.2 K to 140 K for the DMR calculations discussed below. In the following we shall concentrate on explaining the DMR step height defined as $D(140\ \mathrm{K}) - D(4.2\ \mathrm{K})$. The experimental reproducibility of that step height for different samples but the same sample state was at least within ±5%.

Using $A_{dis} = 0.21$ (calculated from equation (2) having $R_H^{4.2}(\mathrm{dis}) = -6.90$); $A_{ph} = 1$, which corresponds to $R_H^{300}(\mathrm{ph}) = 5.1$; ρ_d as from figure 2 and ρ_{ph} according to the undeformed reference sample we obtain by equation (3) ('Barnard's version', $b = 0.257$) the dashed curves shown in figure 2. They have a step height about 50% less than the measured curves. Attempts to fit directly the measured DMR curves by equation (3) with only A_{dis} as fitting parameter and $A_{ph} = 1$ yield values of $A_{dis} \sim 0.11$–0.12, whereas from $R_H^{4.2}(\mathrm{dis})$ the direct value 0.21 is calculated. Otherwise a change of A_{ph} from the value of unity to a value of about 1.4 would give agreement between measured and calculated DMR curves, but then we would not have $R_H^{300}(\mathrm{ph})$ correct.

A possible reason for the inconsistency of DMR and R_H is that there is a substantial contribution to DMR of different origin than scattering anisotropy. Alternatively the discrepancy may originate because, though equation (3) is an exact formulation of the TGM in the relaxation time approximation, equation (2) is not. The numerical values in (2) were obtained by a fit to certain data, and may well be inappropriate. We consider this matter in the following section.

3.3. Critique and improvement of the two-group model

If the exact distribution of the electronic transport relaxation time $\tau(k)$ is known as a function of wave vector k, R_H can be calculated for cubic metals by the Tsuji formula [25]

$$R_H = \frac{12\pi^3}{e}\left(\int \tau^2(k)v^2(k)\kappa(k)\,\mathrm{d}S\right)\Big/\left(\int \tau(k)v(k)\,\mathrm{d}S\right)^2 \tag{4}$$

where $v(k)$ is the Fermi velocity, $\kappa(k)$ the mean curvature on the Fermi surface and $\mathrm{d}S$ an element of the Fermi surface (the dependence on k will not be specified in the following). Since no exact distribution of $\tau(k)$ is known for any scatterer concerning electrical resistance and LFHE†, equation (4) facilitates estimation of $\tau(k)$ by formulating it in the TGM [10]

$$R_H = \frac{12\pi^3}{e}\left((\tau_B^\kappa)^2\int_B \kappa v^2\,\mathrm{d}S + (\tau_N^\kappa)^2\int_N \kappa v^2\,\mathrm{d}S\right)\Big/\left(\tau_B\int_B v\,\mathrm{d}S + \tau_N\int_N v\,\mathrm{d}S\right)^2 \tag{5}$$

where τ_B^κ, τ_N^κ, τ_B and τ_N are (constant) mean relaxation times for the 'groups' of neck and belly electrons. The main point is that in the case of the LFHE the averaging process

† In general relaxation times obtained by the de Haas–van Alphen effect are not reliable for DMR and LFHE [4, 24]. The situation is similar in the case of magnetic field induced surface state resonance [26].

is different in the numerator and denominator of equation (4) since the squared relaxation times are weighted by the curvatures in the numerator. The TGM makes no distinction between these two averages and thus arrives from (5) at equation (1), where

$$a = \left(\int_N v^2\kappa\,dS\right)\Big/\int_B v^2\kappa\,dS$$
$$b = \left(\int_N v\,dS\right)\Big/\int_B v\,dS \tag{6}$$
$$f = \frac{12\pi^3}{e}\left(\int_B v^2\kappa\,dS\right)\Big/\left(\int_B v\,dS\right)^2.$$

To be precise

$$\tau_N = \left(\int_N v\tau\,dS\right)\Big/\int_N v\,dS \qquad \tau_B = \left(\int_B v\tau\,dS\right)\Big/\int_B v\,dS \tag{7}$$

and

$$(\tau_N^\kappa)^2 = \left(\int_N v^2\tau^2\kappa\,dS\right)\Big/\int_N v^2\kappa\,dS \qquad (\tau_B^\kappa)^2 = \left(\int_B v^2\tau^2\kappa\,dS\right)\Big/\int_B v^2\kappa\,dS. \tag{8}$$

We may write equation (5) as follows:

$$R_H = \frac{12\pi^3}{e}s\left[\left(\int_B v^2\kappa\,dS\right)\Big/\left(\int_B v\,dS\right)^2\right]$$
$$\times\left[1+\frac{r}{s}A^2\left(\int_N v^2\kappa\,dS\right)\Big/\int_B v^2\kappa\,dS\right]\Big/\left[1+A\left(\int_N v\,dS\right)\Big/\int_B v\,dS\right]^2 \tag{9}$$

where

$$r = (\tau_N^\kappa)^2/\tau_N^2 \qquad s = (\tau_B^\kappa)^2/\tau_B^2 \qquad A = \tau_N/\tau_B.$$

Equation (9) is only equal to (1) if $r = s = 1$. Equation (9) is exact insofar as equation (4) is exact and should be able to give better agreement with the A values needed for the calculation of the DMR according to equation (3). Even though the numbers r and s are not known and are not accessible by experiment, nevertheless an improvement of the TGM can be achieved considering equation (9). Since the curvature on the belly does not change as much as on the neck s is likely to much closer to unity than r. r/s is very difficult to estimate, but we can eliminate r/s by choosing a neck angle that gives $(\int_N v^2\kappa\,dS)/(\int_B v^2\kappa\,dS) = 0$. This condition defines a neck angle of 18.7° for copper and reduces equation (9) by using (6) to

$$-R_H = sf/(1+Ab)^2 \tag{10}$$

with $f = 7.34\times10^{-11}$ m^3 C^{-1}, $b = 0.219$ and $a = 0$ based on the precise Fermi surface data of Halse [27]. The values of the terms f and b with $a = 0$ were calculated by Watts [28]. Equation (10) is still exact and has the advantage that the stronger correction (r/s)

does not appear. We now have two adjustable parameters s and A. Furthermore s should be close to unity because the mean curvature of the belly will not deviate much from that of a sphere.

A change of $b = 0.257$ to $b = 0.219$ does not have much influence on the description of the DMR by equation (3). The direct fits of the experimental DMR curves as performed in subsection 3.2 but now only changing b to 0.219 gives practically the same result as before, $A_{dis} \sim 0.11 \pm 0.005$, having taken into account an error of $\pm 5\%$ of the experimental step height. However, now in the 'exact version' of equation (10) the same value, $A_{dis} \sim 0.11 \pm 0.005$, can also be obtained from $R_H^{4.2}(\text{dis}) = 6.90$ if $s = 0.986 \pm 0.002$ is used, which is close to unity, as expected. Taking into account a measuring error of $R_H^{4.2}(\text{dis})$ of ± 0.07 increases the error in s to ± 0.012. Furthermore the 'exact version' (10) describes consistently $R_H^{300}(\text{ph}) = 5.0$–$5.1$ with $A_{ph} = 1$ and $s = 1.0024$–1.022. The increase of the term f by 1% due to lattice expansion from the temperature 4.2 K to 300 K has been taken into account.

Even when putting $s = 1$ in our 'exact version' of the TGM we obtain significantly better results than in the Barnard version. Then from $R_H^{4.2}(\text{dis}) = 6.90 \pm 0.07$ (1% error) one obtains $A_{dis} \sim 0.14 \pm 0.02$ (14% error, see below). Doing a similar DMR calculation as in subsection 3.2 (equation (3)) but now using $A_{dis} \sim 0.14 \pm 0.02$ and $b = 0.219$ ($A_{ph} = 1$, ρ_{ph} and ρ_d unchanged) we obtain the full lines in figure 2, where the error bar (only drawn at 130 K) is due to the experimental uncertainty of A_{dis} obtained from $R_H^{4.2}(\text{dis})$. These curves show much better agreement with the experimental points, which shows that the correction of the TGM—as shown above—works in the right direction. Furthermore direct fits of the experimental curves by equation (3) with only A_{ph} as fitting parameter and having $s = 1$, $A_{dis} = 0.14 \pm 0.02$ and $b = 0.219$ require now $A_{ph} \sim 1.13 \pm 0.11$, which is much closer to isotropic electron–phonon scattering than the value $A_{ph} = 1.40$ due to the similar fit in the Barnard version (see subsection 3.2).

The present calculations show that a very small change in R_H produces a large change in the fitted value of A_{dis}, e.g. in copper a 1% change in the experimental value of $R_H^{4.2}(\text{dis})$ produces about 14% change in A_{dis}. This is a special situation for the case of dislocations in copper due to the term $Ab \ll 1$ in equation (10). Consequently $R_H^{4.2}(\text{dis})$ has to be measured with very high accuracy.

4. Conclusions

The improved TGM *can* explain consistently the DMR step height and the low-field Hall coefficient of dislocated high-purity copper. There is no reason to take into account other sources of DMR beside scattering anisotropy. The analysis shown agrees with isotropic electron–phonon scattering between 130 K and room temperature ($A_{ph} = 1$). In contrast electron–dislocation scattering is extremely anisotropic ($A_{dis} \sim 0.1$). Investigations are currently being done in silver and gold to see whether our improved TGM works there.

Acknowledgments

The author thanks M Müller for his contribution of sample preparation and DMR measurements. The kind support of M Müller, V Gröger, M Zehetbauer and B R Watts and their helpful discussions are gratefully acknowledged. This work has been supported by the Fonds zur Förderung der wissenschaftlichen Forschung under project 9930-PHY.

References

[1] Rabier J, George A, Bréchet Y and Kubin L (ed) 1994 *Proc. Dislocations 93 (Aussois); Solid State Phenom.* **35–36**
[2] Müller M, Zehetbauer M, Sachslehner F and Gröger V 1994 *Solid State Phenom.* **35–36** 557
[3] Gantmakher V F and Levinson Y B 1987 *Modern Problems in Condensed Matter Sciences* vol 19, ed V M Agranovich and A A Maradudin (Amsterdam: North-Holland)
[4] Watts B R 1989 *Dislocations in Solids* vol 8, ed F R N Nabarro (Amsterdam: Elsevier)
[5] Zehetbauer M 1989 *J. Phys.: Condens. Matter* **1** 2833
[6] Watts B R 1988 *J. Phys. F: Met. Phys.* **18** 1197
[7] Bross H and Häberlen O 1993 *J. Phys.: Condens. Matter* **5** 7687
[8] Dugdale J S and Basinski Z S 1967 *Phys. Rev.* **157** 552
[9] Ziman J M 1960 *Electrons and Phonons* (Oxford: Clarendon)
[10] Dugdale J S and Firth L D 1969 *J. Phys. C: Solid State Phys.* **2** 1272
[11] Barnard R D 1977 *J. Phys. F: Met. Phys.* **7** 673
[12] Barnard R D 1980 *J. Phys. F: Met. Phys.* **10** 2251
[13] Sakamoto I and Yonemitsu K 1987 *Japan. J. Appl. Phys.* **26** (Supplement 26–3) 645
[14] Lengeler B and Papastaikoudis C 1980 *Phys. Rev.* B **21** 4368
[15] Baratta A J and Ehrlich A C 1983 *Phys. Rev.* B **28** 4136
[16] Müller M 1994 *Thesis* Universität Wien
[17] Zürcher R, Müller M, Gröger V and Zehetbauer M 1994 to be published
[18] Sachslehner F and Vodel W 1992 *Cryogenics* **32** 805
[19] Gröger V and Stangler F 1977 *Acta. Phys. Austriaca* **46** 197
[20] Lengeler B, Schilling W and Wenzl H 1970 *J. Low-Temp. Phys.* **2** 59
[21] Matula R A 1979 *J. Phys. Chem. Ref. Data* **8** 1147
[22] Zehetbauer M, Gröger V and Watts B R 1991 *Solid State Commun.* **79** 465
[23] Andrews P V, West M B and Robeson C R 1969 *Phil. Mag.* **19** 887
[24] Springford M 1971 *Adv. Phys.* **20** 493
[25] Tsuji M 1958 *J. Phys. Soc. Japan* **13** 979
[26] Simanek D E, Baratta A J, Lodder A and Ehrlich A C 1987 *Phys. Rev.* B **36** 9082
[27] Halse M R 1969 *Phil. Trans. R. Soc.* A **265** 507
[28] Watts B R 1994 Private communication